International Journal of Innovative Computing, Information and Control
Volume **12**, Number **4**, August **2016**

ICIC International ©2016 ISSN 1349-4198
pp. 1165–1178

THEORETICAL DERIVATION AND EXPERIMENTAL STATISTICAL ANALYSIS ON RADIAL VASCULAR MECHANICAL MODELING WITHIN THE EFFECTS OF HYPERTENSION

Jieyi Zhu[1,2], Changan Zhu[1] and Yining Sun[1,2,*]

[1]Department of Precision Machinery and Precision Instrumentation
University of Science and Technology of China
No. 96, Jinzhai Road, Baohe District, Hefei 230026, P. R. China
zhujieyi@mail.ustc.edu.cn

[2]Research Center for Information Technology for Sports and Health
Institute of Intelligent Machines
Chinese Academy of Sciences
Science Island, Hefei 230031, P. R. China
*Corresponding author: ynsun@iim.ac.cn

Received February 2016; revised June 2016

Abstract. *This paper presents a theoretical analysis of radial vascular modeling and discusses the effects of hypertension, providing experimental and statistical data for demonstration. We develop a mathematical model of the relationship between blood pressure and the elasticity modulus of vessels. A simulation of fluid-structure interaction is given for theoretical analysis. From the theoretical model, we deduced the equation for radial waveform signal reconstruction. We also experimentally measured radial pressure waveform data, and collected radial waveform signals from 72 patients, including normal and hypertension patients. Our system conducted waveform signals acquisition, from which we can then build analysis radial waveform signals for individuals with different blood pressure levels. In our sample, we analyze patients' waveforms with systolic pressures ranging from 90 mmHg to 160 mmHg. We compare the theoretical results with the experimental measurements, and find our proposal that blood pressure has a correlative relationship with the vessel elasticity is supported.*

Keywords: Radial waveform, Mechanical modeling, Waveform reconstruction, Blood pressure

1. **Introduction.** Research into central arterial pressure is increasingly relevant to the study of cardiovascular diseases. Direct measurement with an intra-aortic transducer is now the theoretical gold standard for assessing central arterial pressure. However, the technical difficulties of direct measurement have rendered it unachievable in actual clinical practice. It has been instead suggested that aortic pressure can be estimated by transforming peripheral pulse waveforms [1], so central aortic pressure and one type of peripheral pulse waveform can be analyzed together, such as aortic and femoral, aortic and carotid, aortic and radial [2], and finger and brachial. In actual measurements, radial artery waveforms can be easily obtained by an applanation tonometry instrument, applying an Omron HEM-7012 on the radial artery of the left arm [3]. Studies have found that pulsatile pressure and flow waveforms can provide important information on cardiovascular diseases, including diabetic mellitus, hyperlipidemia, and hypertension [4]. From the obtained radial waveforms we can therefore analyze the specific effects of a cardiovascular disease on the physiological characteristics of the patients' radial vascular vessels [5]. In this study, we analyze the effects of hypertension on the radial vascular

characteristics and its waveforms. The mechanical modeling of radial vascular vessels enables us to further understand the mathematical relationship between blood pressure and vascular elasticity, using the theoretical derivation and biomechanical simulation [6]. We also collect and process actual radial waveforms from normotensive and hypertension patients with systolic pressures ranging from 90 mmHg to 160 mmHg, and discuss the experimental statistical relationship. The theoretical analysis and experimental discussion are then compared to demonstrate the relationship between blood pressure and radial vessel elasticity.

For mechanical modeling, we consider the radial vascular vessel as a single hollow micro-cylindrical tube, with blood flowing inside the channel. The highest fluid pressure in the channel is the systolic pressure of the blood as it flows through the radial artery. The lowest pressure of this same blood is the diastolic pressure during one cycle. Although there are some numerical techniques efficient for solving complex partial equations such as element free methods [7], we deduce the explicit formulation of the relationship between blood pressure and vascular elasticity from present simple hemodynamic model [8]. Fluid-structure interaction is necessary for mechanical simulation when analyzing the effects of blood pressure on the radial vascular vessels [9]. Ansys software is applicable for this fluid-structure simulation [10]. We measured 72 subjects during our experiment, including hypertension patients. We divided the subjects into different subgroups according to their systolic pressure period, and extracted their one-cycle radial waveforms. We completed the waveform reconstruction by mathematically matching for different blood pressures, adjusting for parameters such as age and sex. The theoretical model and the experimental discussion are then normalized to investigate the association between blood pressure and radial vessel elasticity.

In summary, we conduct both theoretical and experiment research on the radial vascular mechanical modeling within the effects of hypertension. In the theoretical research, the mechanical modeling of radial vascular is modeled and the simulation is finished. In the experimental research, the statistical analysis of 72 patients' pressure waveform is compared with the theoretical research, studying the effects of hypertension on radial waveforms.

2. **Radial Vessel Mechanical Model.** To analyze the theoretical relationship between blood pressure and radial artery visco-elasticity strain/stress, it is necessary to examine the radial artery mechanical model. If we consider the blood behavior in a radial segment of a human artery as a one-dimensional, Newtonian, incompressible fluid flow inside an elastic tube, we can deduce the flow quantity expression from a continuity equation:

$$\frac{\partial Q}{\partial z} + \frac{\partial A}{\partial t} = 0 \tag{1}$$

where A is the cross-sectional area, Q is a flow (volume/time) through the elastic tube, and z is the axial direction. According to Bergman et al. [11], the pulsatile flow of an incompressible fluid in a rigid, straight circular cylinder is considered as a system of the Cauchy equation of motion reduction:

$$\rho \frac{\partial u}{\partial t} = -\frac{\partial P}{\partial z} + \frac{1}{r}\frac{\partial (rT)}{\partial r} \tag{2}$$

In this equation, ρ is the fluid density, u is the axial velocity of the flowing fluid, P is the dynamic pressure of the flowing fluid, r and z are the radial and axial coordinates respectively, t is the calculus time for computing physical variables' changes over time, and T is the shear stress in the axial direction.

For expressing the shear stress in a rheological model, T is a function of the strain rate in a Newtonian model, and the viscosity μ is therefore regarded as the absolute viscosity, so T can be deduced in (3):

$$T = \mu \frac{\partial u}{\partial r} \tag{3}$$

We use Equation (3) to replace the T in Equation (2), and the linearized momentum equation is given in (4):

$$\rho \frac{\partial u}{\partial t} = -\frac{\partial P}{\partial z} + \mu \left(\frac{\partial^2 u}{\partial r^2} + \frac{1}{r} \frac{\partial u}{\partial r} \right) \tag{4}$$

If the model is under the condition where the radial and tangential motion of fluid is neglected, the pressure gradient can be expressed as the form in Equation (5):

$$-\frac{\partial P}{\partial z} = P_0 \cdot e^{i\omega t} \tag{5}$$

Combining the three Equations (1), (2), and (5) into a joining equation, we obtain the solution, which is already represented in Womersley's paper [12], and is shown in (6):

$$u = u(r, z, t) = \frac{A}{i\omega\rho} \left[1 - \frac{J_1 \left(i^{1.5} \alpha y \right)}{J_0 \left(i^{1.5} \alpha \right)} \right] e^{i\omega t} \tag{6}$$

In this solution $\alpha = (\omega\rho/\mu)^{0.5} r_0$, $y = r/r_0$, r_0 is the internal arterial radius, and J_0 and J_1 are zero and first order, respectively, from the Bessel functions of the first kind.

Thus, as u is the axial velocity of the flowing blood, we can calculate the volumetric flow rate Q from the integral from 0 to r, and the equation is deduced in (7):

$$Q(t) = \int_0^r u(r, z, t) 2\pi r dr = \frac{A_0}{i\omega t} \cdot \frac{\partial P}{\partial z} (1 - F_{10}) \tag{7}$$

In Equation (7), $F_{10} = J_1 \left(i^{1.5} \alpha y \right) / J_0 \left(i^{1.5} \alpha \right)$, and $A_0 = \pi r_0$ (A_0 and r_0 are the initial cross-sectional area and the initial radius of the discussed radial vascular vessel). Following the above formula derivation, we can create a schematic diagram for the radial artery configuration, shown in Figure 1. Figure 1 represents the model of radial artery vascular, the red cylinder inside stands for the blood flowing in the vessel, and the grey cylinder outside stands for the artery wall. Figure 1 also marks the radial coordinate r and the axial coordinate z, which is used in Equation (2). This figure could be able to describe the rigid model of the radial artery mechanical modeling. This model is an ideal model for radial artery mechanical analysis. However, if we want to consider the blood as flowing stream, the model needs to be modified as fluid-structure model. In the latter part of this chapter, we would discuss the fluid model.

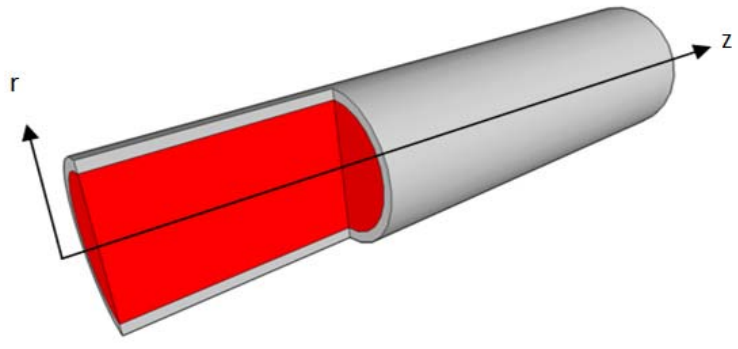

FIGURE 1. The schematic diagram for radial artery configuration

From the mathematical modeling of a human left arm radial artery, the volumetric flow rate Q can be calculated as the difference between the arriving and the reflection flow. The arriving flow can be calculated as (8):

$$Q_f = Q(\omega, 0, t) = Q_0 e^{i\omega t} \tag{8}$$

If we consider the reflection to occur at the branching point of the radial artery, the total flow is calculated as (9):

$$Q = Q_f - Q_r = Q_0 e^{i\omega t} \left(1 - Ce^{-2ikl}\right) \tag{9}$$

Based on the relationship between the flow rate and the blood pressure, the pressure of the arriving flow can be written as a real part in (10):

$$P_f = P(\omega, 0, t) = P_0 e^{i\omega t} \tag{10}$$

According to the reference for calculating the reflection's influence on the total pressure [13], the total pressure at the pulse point at the radial artery is calculated as (11):

$$P = P_0 e^{i\omega t} \left(1 + Ce^{-2ikl}\right) + P_0 e^{i\omega t} C' e^{-2ikl_t} + P_1 \tag{11}$$

where P_1 is the sum of all re-reflected waves, l_t is the distance between the pulse point and the beginning point of the vessel terminal, and $P_0 e^{i\omega t} C' e^{-2ikl_t}$ is the terminal resistance backward wave.

Considering the fluid model in the bloodstream, the flow in this study is assumed to be laminar, Newtonian, viscous, and incompressible. The blood flow is governed by the Navier-Stokes equations of incompressible flow blood on a moving domain [14]. Combining the Navier-Stokes equations and the continuity equations, the governing equations are shown in Equations (12) and (13):

$$\frac{\partial \overrightarrow{V}}{\partial t} + \overrightarrow{V} \cdot \overrightarrow{\nabla} \overrightarrow{V} + \frac{\overrightarrow{\nabla} p}{\rho} - 2\frac{\eta}{\rho} \overrightarrow{\nabla} \cdot D = \overrightarrow{0} \tag{12}$$

$$\nabla \cdot \overrightarrow{V} = 0 \tag{13}$$

where V is the fluid velocity, P is fluid pressure, ρ is density, η is dynamic viscosity, $\overrightarrow{\nabla}$ is the gradient operator and D is the fluid rate of deformation tensor.

3. Experimental Process.

3.1. **Subjects.** A population of 72 subjects between 25 to 85 years old was recruited from a health screen center, and was initially measured. All the patients' waveforms were measured and recorded in the exercise intervention clinic of Chinese PLA hospital. These patients mainly came from the north provinces of China, such as Beijing, Shandong, and Shanxi. Subjects with irregular heart rhythm, heart failure, and significant cardiovascular disease were excluded according to the questionnaire. Hypertension is defined as a systolic blood pressure $\geq$ 140 mmHg, or diastolic blood pressure $\geq$ 90 mmHg. Our experiment sample included hypertension patients, and details are given in Table 1. Our study focuses on circumstances where varying systolic blood pressure leads to specific radial waveforms characteristics. The systolic blood pressure of the chosen sample therefore ranges widely, with small variations of other factors, such as age, heart rate, and diastolic blood pressure. The hypertension population are all of the condition where systolic blood pressure $\geq$ 140 mmHg.

TABLE 1. Characteristics of the study population ($n = 72$)

Characteristics	Mean ± SD	Range
Male	31 (43.1%)	
Hypertension	16 (22.2%)	
Age (years)	51 ± 2.6	24-84
Height (cm)	162.6 ± 7.1	150-180
Weight (kg)	62.6 ± 9.7	40-84
SBP (mmHg)	127.1 ± 23.0	105-158
DBP (mmHg)	73.9 ± 8.4	60-95
HR (beats/min)	70.4 ± 3.8	65-73

3.2. **Study protocol.** All measurements were performed in air-conditioned environments (22-26°C). Each subject rested for at least 10 minutes before measurements. Measurements were taken in a temperature-controlled room between 8:30 and 11:00 AM. All measurements were obtained after 12 h fasting. No consumption of alcohol was allowed for 24 h, and no tea, coffee, or smoking for 8 h before the examination. For each patient, systolic blood pressure (SBP) and diastolic blood pressure (DBP) were measured three times on the left arm with an Omron HEM-7012 (Omron Healthcare, Japan). Mean arterial pressure was calculated as one third of pulse pressure added to DBP. All measurements were performed by the same operator and conducted in the supine position, and recorded by Hu as the measurement reference [15]. Based on the methods and techniques established in the study, we developed arterial stiffness detector (BX-CFTI-200) and non-invasive central arterial pressure analyzer (BX-CAP-100), and demonstrated them in the exercise intervention clinic of Chinese PLA hospital. BX-CAP-100 records radial pulse waveform using applanation tonometry and obtains central arterial pressure waveform by the transformation of GTF. Pulse wave analysis was then applied to extracting a number of hemodynamic index, including central SBP, AI and SEVR. This equipment has cheap cost and is easy to operate, satisfying the requirement of patient waveforms obtainment.

3.3. **Pressure waveforms acquisition and process.** Applanation tonometry was simultaneously applied on the carotid and radial artery. Carotid tonometry measurements are used as reference for the central BP, and the carotid tonometer-derived SBP in itself has been shown to be on average 1.8 mmHg higher than the invasive central pressure [16]. To obtain an optimal waveform, 10 seconds of consistent radial arterial waveforms were recorded and then calibrated using the measured brachial SBP and DBP. Pressure upstroke, the first and second systolic peaks, and the diastolic peak were detected using algorithms based on multidimensional derivatives. Central blood pressure (CBP) was calculated as the pressure of the second systolic peak. Half the time interval between the first and second systolic peaks is calculated to estimate the pulse transit time (PTT). AI were calculated as AI = (P2 – DBP)/(SBP – DBP). Details of the computation method were presented in a previous study. DBP is the diastolic blood pressure, SBP the systolic blood pressure, P3 the third systolic blood pressure, and P2 the second systolic blood pressure. Figure 2 shows the radial waveform within one cycle.

Totally we measured 72 patients, and the systolic blood pressure of the patients in our sample range from 90 mmHg to 160 mmHg. For the hypertension waveform analysis, we subdivided the sample into four subgroups, Group 1: systolic blood pressure <= 110 mmHg, Group 2: 110 mmHg < systolic blood pressure <= 125 mmHg, Group 3: 125 mmHg < systolic blood pressure <= 140 mmHg, Group 4: 140 mmHg < systolic blood pressure. Group 1 had 11 patients, Group 2 had 23 patients, Group 3 had 22 patients, and

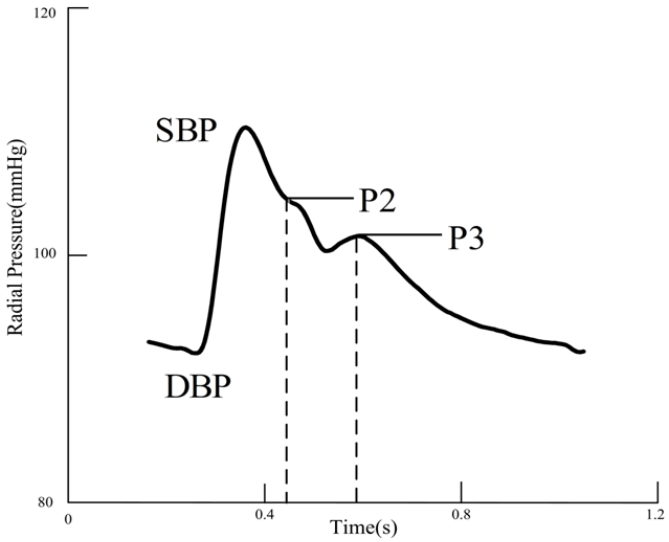

FIGURE 2. Schematic diagram for the radial waveform of pulse waves within one cycle

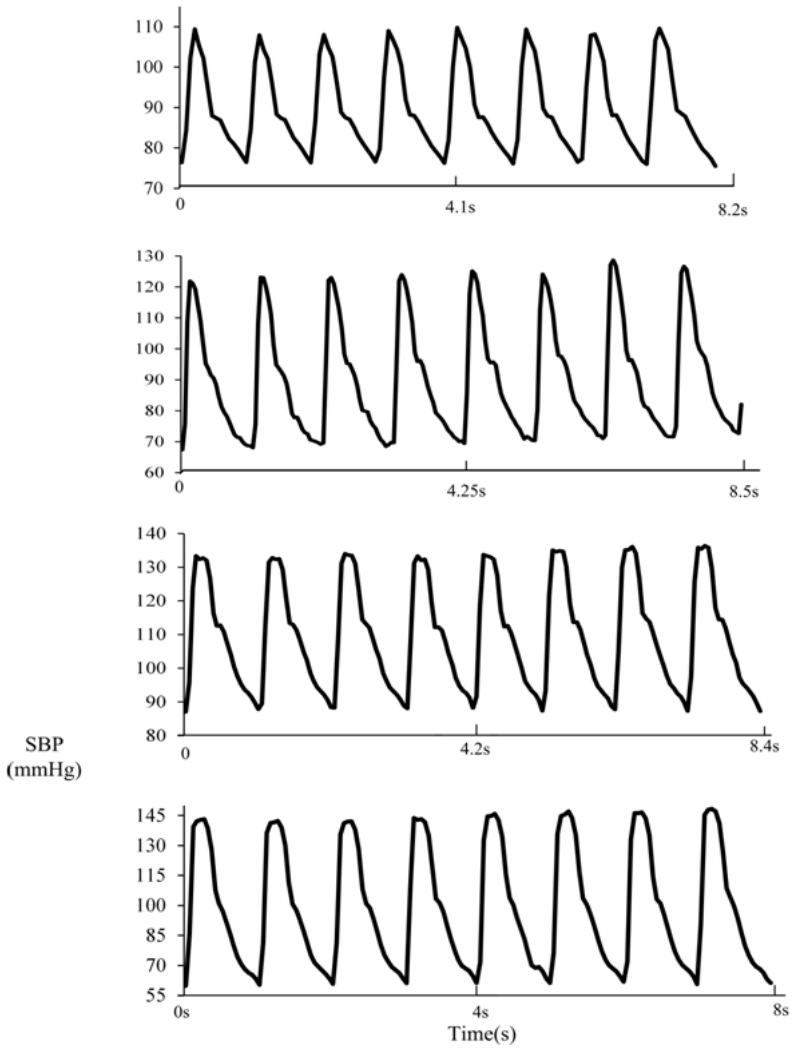

FIGURE 3. The segment within eight cycles of the radial pulse waveforms for the four groups

Group 4 had 16 patients. In our sample, all the patients had heart rates of around 70, and the standard deviation is ±3.8, so we adjusted the waveforms of all patients to obtain the average one-cycle length. We recorded all the patients' waveform signals, and calculated the average waveform for each group. The recorded averaged waveforms for all four groups are shown in Figure 3. At first, the recorded waveforms were eight-cycle waveforms within 8-8.5 s. Then the one-cycle waveform was extracted out from the eight-cycle waveforms.

In later analysis, the radial pulse waveform within one cycle was extracted from the eight-cycle waveform segment of each group. In the next chapter, we will discuss the characterization of one cycle average waveform from Groups 1 to 4, as systolic blood pressure increases from below 110 mmHg to above 140 mmHg.

3.4. **Simulation.** Combined with the theoretical derivation of radial artery waveforms, mechanical simulation can be completed using Ansys software. We consider the radial artery vessel as a long cylinder model with blood flowing inside the inner chamber. The radial artery consists of three components: intima, media, and adventitia. As provided by [17], the parameters of the layers are given in Table 2.

TABLE 2. Mechanical properties of the three-layer model

	E (Pa)	ν	R (m)
Intima	3.856×10^5	0.45	0.0107
Media	1.157×10^6	0.45	0.0119
Adventitia	3.856×10^5	0.45	0.0125

After inputting the mechanical properties of the radial artery, the fluid property of the flowing blood was also considered. The blood has a density of 1000 kg/m^3, sharing the inner diameter 0.0105 m. In our Ansys simulation, we attempted to simulate the condition during the systolic period throughout the whole cycle. The systolic blood pressure units must therefore be converted into Pascal (Pa) from millimeter of mercury (mmHg). Millimeter of mercury refers to the pressure of 1 mm deep mercury, so the conversion is P = 1mmHg = $13.6 \times 1000 \times 9.8 \times 0.001$ Pa = 133.28 Pa. The pressure 100 mmHg is then 13328 Pa, and the pressure of 150 mmHg is 19992 Pa. In our simulation, we set the blood pressure during the systolic period as 100 mmHg. The Ansys auto-calculation of the stress contour of the radial artery is shown in Figure 4.

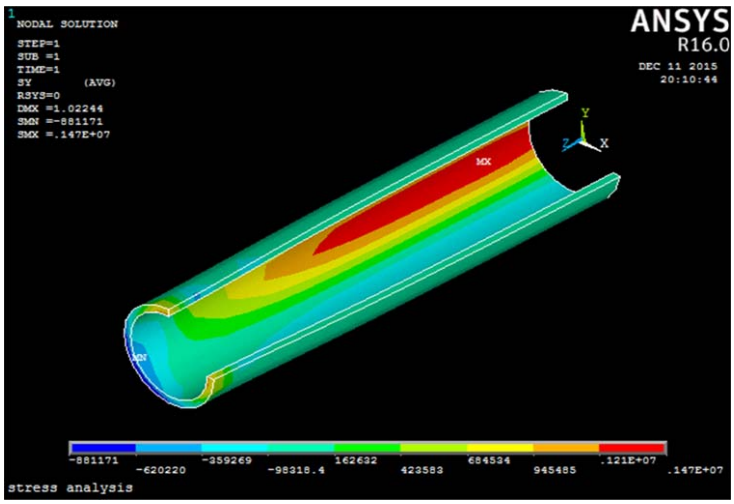

FIGURE 4. The Ansys simulation contour for 100 mmHg systolic blood pressure

4. Waveform Reconstruction.

4.1. **Radial waveform theoretical basis.** It has been reported that the radial pulse waveforms could be estimated and modeled by Gaussian functions [18]. We use three Gaussian functions to conduct the radial waveform curve fitting, referred to as $f_1(n)$, $f_2(n)$, and $f_3(n)$. Each function depends on three parameters: waveform height H_k, half-width W_k, and center position C_k. The Gaussian function equation is described as (14):

$$f_k(n) = H_k \times \exp\left(-\frac{2(n - C_k)^2}{W_k^2}\right) \tag{14}$$

where $n = 1, 2, 3, \ldots, 1000$, $k = 1, 2, 3$, and C_k needs to satisfy the following condition: $1 < C_1 < C_2 < C_3 < 1000$.

When all the parameters of the three Gaussian functions are determined, the H_k, C_k, W_k $(k = 1, 2, 3)$, the superimposed curve $f(n, x)$ of the three functions is regarded as the fitted curve, and the superimposed curve equation is described as (15):

$$f(n, x) = \sum\nolimits_{k=1}^{3} f_k(n) \tag{15}$$

where $x = [H_k, W_k, C_k]$ can be seen as the parameter vector. After examining the fitting results we can analyze the influencing factors on radial pressure waveforms, including age, sex, and hypertension [19].

4.2. **Hypertension waveform analysis.** In our radial waveform analysis, we conducted calculations and curve fitting to research the effects of hypertension on radial artery physiological waveform signal modeling, particularly those of the systolic blood pressure. The systolic blood pressures of the patients in our sample range from 90 mmHg to 160 mmHg. In our calculation, we subdivided the sample into four subgroups, Group 1: systolic blood pressure <= 110 mmHg, Group 2: 110 mmHg < systolic blood pressure < =125 mmHg, Group 3: 125 mmHg < systolic blood pressure <= 140 mmHg, Group 4: 140 mmHg < systolic blood pressure. Details of the four subgroups are given in Table 3.

TABLE 3. The systolic blood pressure periods of the four subgroups

	Systolic blood pressure (mmHg)	Patients numbers
Group 1	< 110	11
Group 2	110-125	23
Group 3	125-140	22
Group 4	≥ 140	16

There are 11 patients with systolic blood pressure under 110 mmHg in Group 1, none of which has hypotension, which is defined as systolic blood pressure under 90 mmHg, or diastolic blood pressure under 60 mmHg. We measured all the patients' radial waveform signals, and selected the waveform the closest to the average. The one cycle length is proximal to the average length, and the average values of all the patients' waveform signals are calculated. The selected radial waveform of Group 1 is shown in Figure 5.

For Group 1, we constructed our matlab program for the carotid-radial transfer function based on the frequency domain, and harmonics are used for waveform reconstruction. According to the corresponding reference, the complete arterial pulse can be described by 10 harmonics at most, and over 95% of the signal energy could be described in the first 5 to 9 harmonics [20]. The first 4 have been found to reliably estimate central blood pressure signals [21], so we selected this for the transfer function, and found that within the 1-4th to 1-10th harmonics was appropriate. From this transfer function we obtained

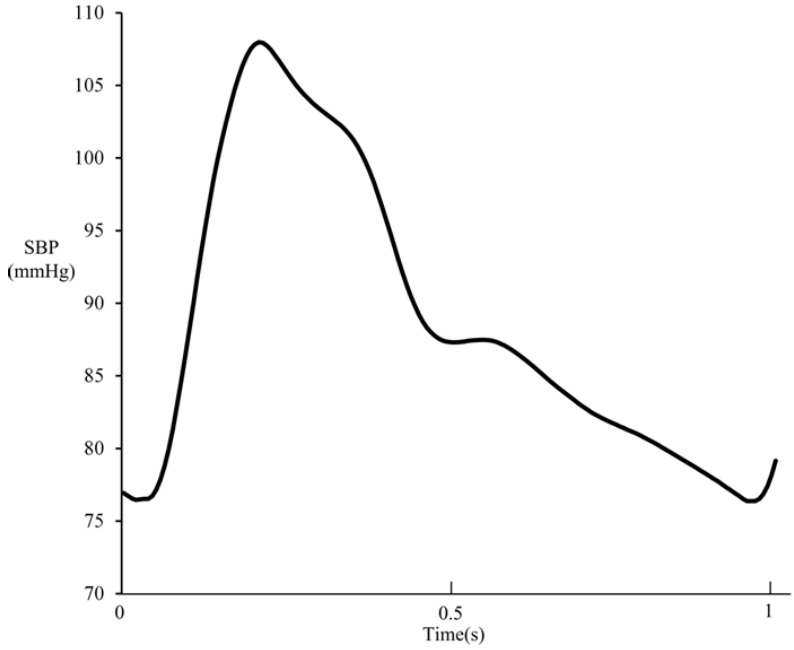

FIGURE 5. The selected average radial waveform of pulse waves within one cycle for Group 1

the matching function of the radial artery waveform, and after residual calculation the function is confirmed as the combination of 10 harmonics shared with the least residual, shown in Equation (16):

$$P_{G1} = P_0 + P_0 C_1 \left(e^{\omega k_1 t} + e^{2\omega k_1 t} + e^{3\omega k_1 t} + \ldots + e^{8\omega k_1 t} + e^{9\omega k_1 t} + e^{10\omega k_1 t}\right) \tag{16}$$

For the fitting function precision calculation, we first calculated the precision for fitting function within different harmonics numbers, and in Group 1 we found the 1-10th harmonics are the most suitable. We then adjusted the fitting parameters C_1 and k_1, attempting to obtain the most appropriate parameter with the least residual.

Group 2 is made up of 23 patients with systolic blood pressure ranging from 110 to 125 mmHg. We measured all the patients' radial waveform signals, and selected the closest to the average waveform. The one cycle length is the closest to the average length, and the average values of all the patients' waveform signals are calculated. The selected radial waveform of Group 2 is shown in Figure 6.

As in Group 1, we used the carotid-radial frequency domain transfer function to calculate the fitting function of Group 2's radial waveform, and after calculating the residual the fitting function with the least residual is as (17):

$$P_{G2} = P_0 + P_0 C_2 \left(e^{\omega k_2 t} + e^{2\omega k_2 t} + e^{3\omega k_2 t} + \ldots + e^{8\omega k_2 t} + e^{9\omega k_2 t} + e^{10\omega k_2 t}\right) \tag{17}$$

Group 3 included 22 patients, with systolic blood pressure ranging from 125 to 140 mmHg. We measured all patients' radial waveform signals, and selected the closest to the average waveform. The cycle length is the nearest to the average length, and the average values of all patients' waveform signals are counted. The representative radial waveform of Group 3 is shown in Figure 7. From Group 3's average waveform, we could find the systolic peak of the average waveform becomes broadened, the length of Group 3's systolic peak is as twice longer as that of Group 2, and even much longer than that of Group 1. It is indicated that perhaps there is some association between the systolic peak length and the value of systolic blood pressure.

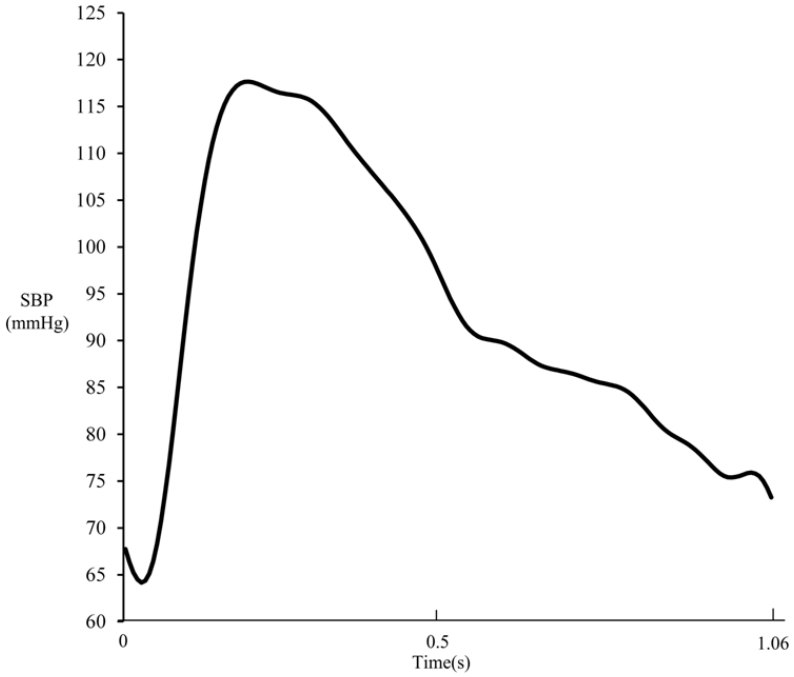

FIGURE 6. The selected average radial waveform of pulse waves within one cycle for Group 2

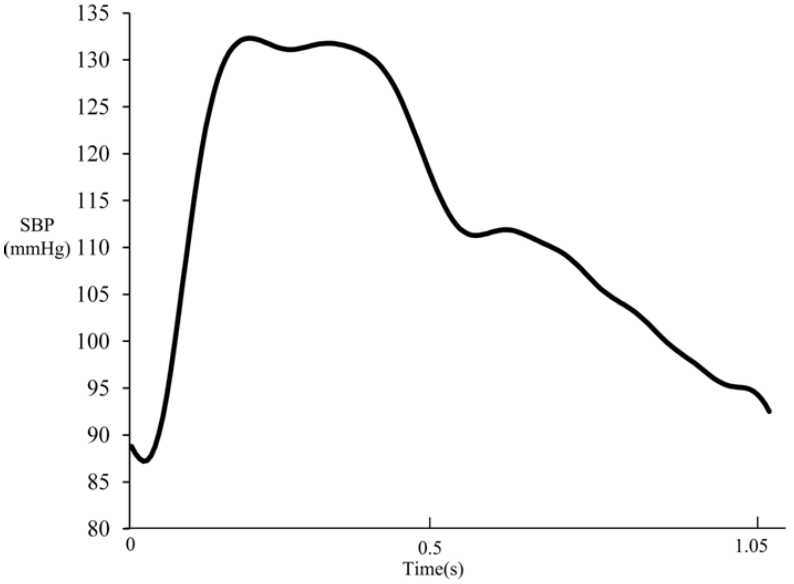

FIGURE 7. The selected average radial waveform of pulse waves within one cycle for Group 3

For Group 3, the appropriate fitting function with the least residual is as (18):

$$P_{G3} = P_0 + P_0 C_3 \left(e^{\omega k_3 t} + e^{2\omega k_3 t} + e^{3\omega k_3 t} + \ldots + e^{7\omega k_3 t} + e^{8\omega k_3 t} \right) \tag{18}$$

Group 4 includes 16 patients with systolic blood pressure above 140 mmHg. As hypertension is defined as systolic blood pressure $\geq$ 140 mmHg, or diastolic blood pressure $\geq$ 90 mmHg, this is therefore a hypertension group, and all patients in it have systolic blood pressure $\geq$ 140 mmHg. We measured all patients' radial waveform signals, and selected the closest to the average waveform. The cycle length is the nearest to the

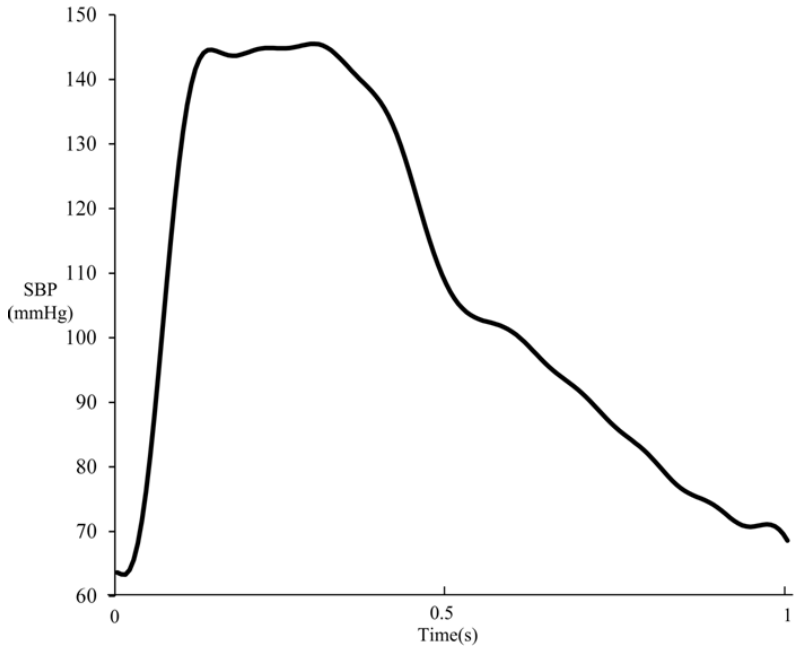

FIGURE 8. The selected average radial waveform of pulse waves within one cycle for Group 4

TABLE 4. The fitting parameter values for the groups

	SBP	C	k
Group 1	105	C_1:1.15	k_1:0.43
Group 2	115	C_2:1.95	k_2:0.51
Group 3	135	C_3:1.65	k_3:0.53
Group 4	155	C_4:2.99	k_4:0.59

average length, and all patients' waveforms are calculated for their average value. The representative radial waveform of Group 4 is shown in Figure 8.

Finally, the most appropriate fitting function we calculated for Group 4 is (19):

$$P_{G4} = P_0 + P_0 C_4 \left(e^{\omega k_4 t} + e^{2\omega k_4 t} + e^{3\omega k_4 t} + \ldots + e^{8\omega k_4 t} + e^{9\omega k_4 t} + e^{10\omega k_4 t}\right) \tag{19}$$

We calculated the two parameters during our fitting process for each group, given in Table 4.

Combining these four groups, we can establish the relationship between the systolic blood pressure value and the parameter k. In our detail analysis, we selected three subjects from each group, whose systolic blood pressure increases by 5 mmHg from one to the next. The overall relationship is then examined as SBP increases from 100 mmHg to 155 mmHg. From a macro perspective, we observed that as systolic blood pressure increases, the systolic blood pressure period widens. Figure 9 gives the tendency when the subject is under a low systolic blood pressure (under 110 mmHg), and the fitting parameter k is below the value of 0.45. When SBP increases the value of k begins to rise. After SBP enters the hypertension threshold (above 140 mmHg), the value of k tends to fluctuate at 0.55. This indicates that the variation of k is probably a reflection of the broadening of systolic width within a whole cycle. It is also suggested that as systolic blood pressure increases, the radial artery's elasticity is enhanced.

4.3. **Statistical analysis.** From the experimental sample chosen, we conducted statistical analysis between the blood vessel elasticity indicator Augmentation Index (AI) and the

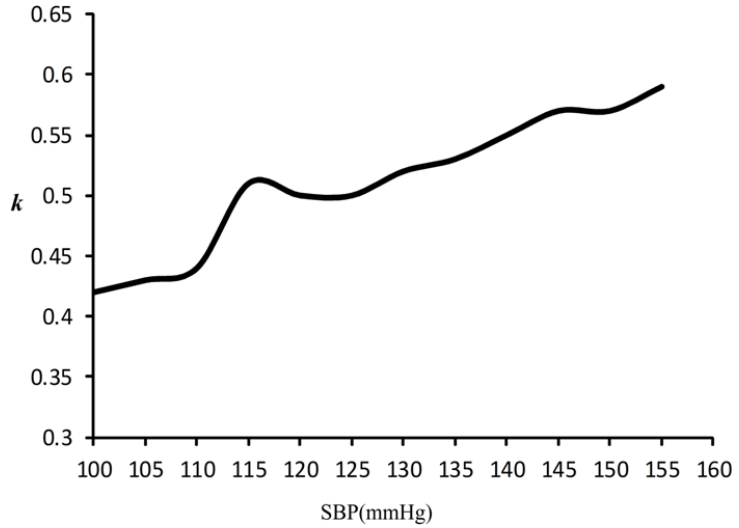

FIGURE 9. The tendency of the fitting parameter k as systolic blood pressure

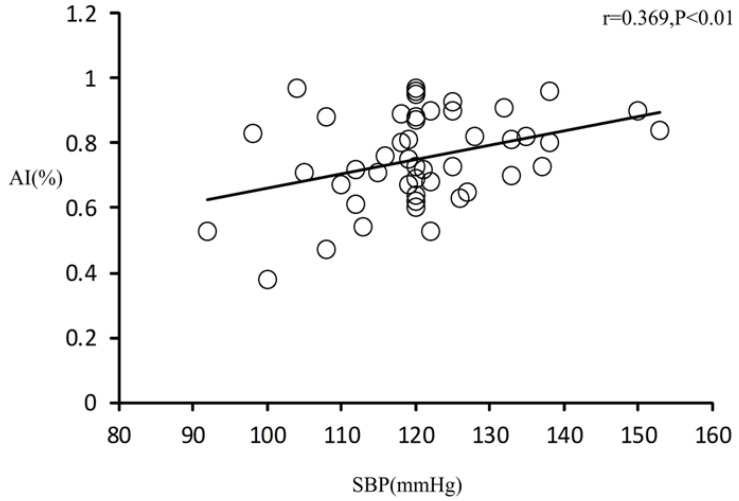

FIGURE 10. The correlation between systolic blood pressure and the Augmentation Index (AI) in our experimental sample

two influencing factors, systolic blood pressure (mmHg) and age (y). Lazovic suggested that age has a subtle influence on radial waveforms [22]. We therefore set the age focus of our sample's members at around 51, with little variation as the standard deviation is 2.6, weakening the influence of age. We conduct two univariate correlation analyses on the Augmentation Index (AI) of systolic blood pressure and on age. These correlation figures are compared and the relationship between the Augmentation Index (AI) and the systolic blood pressure is shown in Figure 10.

In the two correlation figures, we found that in the experimental sample, both systolic blood pressure and age are significantly related to the Augmentation Index (AI). The correlation content between AI and systolic blood pressure is also much higher than that between AI and age. Figure 10 shows that AI is significantly positively correlated with systolic blood pressure ($r = 0.369$, $P < 0.01$). The correlation between AI and age in our experimental group is, however, weak ($r = 0.012$, $P < 0.01$). This comparison suggests that in our sample, the influence of age on radial waveforms is limited. We can therefore discuss the direct effects of hypertension on radial waveforms, as age can be regarded as minor factor.

5. **Conclusions.** In this study, we conducted research on the effects of systolic blood pressure on radial artery waveforms. We started from a mathematical derivation of radial artery flowing blood and blood pressure. We first deduced the theoretical representation of blood pressure, considering the fundamental fluid mechanics principle. Ansys simulation is also carried out to express the stress distribution inside the radial artery vascular vessel when the pressure of blood is applied to the radial blood vessel wall. We completed radial artery waveforms acquisition during our experiment, obtaining waveforms of both normotensive and hypertension subjects. Waveform analysis of each systolic blood pressure period was performed after dividing the overall 72 subjects into four subgroups. In our sample, the subjects chosen had a wide variation of systolic blood pressure, while other factors had little variation. The one-cycle waveform of each group is selected and presented, showing the different characteristics as systolic blood pressure increases from below 110 mmHg to above 150 mmHg. The four groups' radial waveforms were then fitted in a polynomial exponent function, calculating the fitting parameter after statistical analysis. From the tendency of fitting parameter k, we observed that as systolic blood pressure increases, parameter k increases correspondingly. After SBP enters the hypertension threshold, this parameter fluctuates at around 0.55, indicating that as systolic blood pressure increases, the systolic width increases, and it is probable that the radial artery elasticity becomes enlarged.

Acknowledgements. The author sincerely thank research center for information technology of sports and health, institute of intelligent machines, for their system design and data acquisition.

REFERENCES

[1] J. J. Im, R. Wei, Y. C. Lim, C. S. Hwang, H. S. Kim and M. Y. Rheem, Indirect measurement of central pressure using carotid and radial pulses, *International Journal of Bio-Science and Bio-Technology*, vol.5, pp.29-39, 2013.

[2] C.-H. Chen, E. Nevo, B. Fetics, P. H. Pak, F. C. P. Yin, W. L. Maughan et al., Estimation of central aortic pressure waveform by mathematical transformation of radial tonometry pressure: Validation of generalized transfer function, *Circulation*, vol.95, pp.1827-1836, 1997.

[3] M. Nakamura, U. Darhad, Y. Tatsumi, M. Fujioka, A. Kusuhara, H. Maeda and A. Negi, Agreement of rebound tonometer in measuring intraocular pressure with three types of applanation tonometers, *American Journal of Ophthalmology*, vol.142, no.2, pp.332-334, 2006.

[4] P. Saez, E. Pena, M. A. Martinez and E. Kuhl, Computational modeling of hypertensive growth in the human carotid artery, *Computational Mechanics*, vol.53, pp.1183-1196, 2014.

[5] T. Khamdaeng, P. Terdtoon, P. Sakulchangsatjatai and N. Kammuang-lue, The human aortic stiffness determination using the carotid stiffness and pulse wave velocity relation in vivo, *J. Sci. Technol.*, vol.31, pp.710-716, 2012.

[6] A. Das, A. Paul, M. D. Taylor and R. K. Banerjee, Pulsatile arterial wall-blood flow iinteraction with wall pre-stress computed using an inverse algorithm, *BioMedical Engineering*, vol.14, pp.1-19, 2015.

[7] Z. Yang, L. W. Zhang, K. M. Liew and J. L. Yu, Transient analysis of single-layered graphene sheet using the kp-Ritz method and nonlocal elasticity theory, *Applied Mathematics and Computation*, vol.258, pp.489-501, 2015.

[8] P. J. Blanco, S. M. Watanabe and R. A. Feijóo, Identification of vascular territory resistances in one-dimensional hemodynamics simulations, *Journal of Biomechanics*, vol.45, pp.2066-2073, 2012.

[9] Y. Bazilevs, V. M. Calo, Y. Zhang and T. J. R. Hughes, Isogeometric fluid-structure interaction analysis with applications to arterial blood flow, *Computational Mechanics*, vol.38, no.4, pp.310-322, 2006.

[10] C. J. Carmody, G. Burriesci, I. C. Howard and E. A. Patterson, An approach to the simulation of fluid-structure interaction in the aortic valve, *Journal of Biomechanics*, vol.39, no.1, pp.158-169, 2006.

[11] L. E. Bergman, K. J. Dewitt, R. C. Fernandez and M. R. Botwin, Effect of non-newtonian behavior on volumetric flow rate for pulsatile flow of blood in a rigid tube, *Journal of Biomechanics*, vol.4, pp.229-231, 1971.

[12] J. R. Womersley, An elastic tube theory of pulse transmission and oscillatory flow in mammalian arteries, *WADC Technical Report, TR 56-614*, 1957.

[13] B. W. Schaaf and P. H. Abbrecht, Digital-computer simulation of human systemic arterial pulse wave transmission – Nonlinear model, *Journal of Biomechanics*, vol.5, pp.345-364, 1972.

[14] R. Razaghi, A. Karimi, S. Rahmani and M. Navidbakhsh, A computational fluid-structure interaction model of the blood flow in the healthy and varicose saphenous vein, *Vascular*, vol.24, no.3, pp.254-263, 2015.

[15] F. S. Hu, Y. L. Zhang, Z. C. Ma, Q. Q. Cao, Y. B. Xu, Z. J. He et al., A region-matching method for pulse transit time estimation: Potential for improving the accuracy in determining carotid femoral pulse wave velocity, *Journal of Human Hypertension*, vol.29, pp.675-682, 2015.

[16] L. M. van Bortel, E. J. Balkestein, J. J. van der Heijden-Spek, F. H. Vanmolkot, J. A. Staessen, J. A. Kragten et al., Non-invasive assessment of local arterial pulse pressure: Comparison of applanation tonometry and echo-tracking, *Journal of Hypertension*, vol.19, pp.1037-1044, 2001.

[17] A. El Baroudi, F. Razafimahery and L. Rakotomanana, Fluid-structure interaction within three-dimensional models of an idealized arterial wall, *International Journal of Engineering Science*, vol.84, pp.113-126, 2014.

[18] C. Liu, D. Zheng, A. Murray and C. Liu, Modeling carotid and radial artery pulse pressure waveforms by curve fitting with Gaussian functions, *Biomedical Signal Processing and Control*, vol.8, pp.449-454, 2013.

[19] C. Liu, L. Zhao and C. Liu, Effects of blood pressure and sex on the change of wave reflection: Evidence from Gaussian fitting method for radial artery pressure waveform, *Plos One*, vol.9, no.11, pp.1-7, 2014.

[20] P. A. Alberto, B. Mark and W. Andrew, Arterial blood pressure measurement and pulse wave analysis – Their role in enhancing cardiovascular assessment, *Physiological Measurement*, vol.31, pp.R1-R47, 2010.

[21] J. E. Sharman, R. Lim, A. M. Qasem, J. S. Coombes, M. I. Burgess, J. Franco et al., Validation of a generalized transfer function to noninvasively derive central blood pressure during exercise, *Hypertension*, vol.47, pp.1203-1208, 2006.

[22] B. Lazovic, S. Mazic, D. Zikich and D. Zikic, The mathematical model of the radial artery blood pressure waveform through monitoring of the age-related changes, *Wave Motion*, vol.56, pp.14-21, 2015.